Elucidating the electrochemical reaction mechanism of lithium-rich antiperovskite cathodes for lithium-ion batteries as exemplified by $(Li_2Fe)SeO$.

Lennart Singer[a,**], M.A.A. Mohamed[b,d,**], Henrik Hahn[a], Ignacio G. Gonzalez-Martinez[b], Martin Hantusch[b], Karolina Wenelska[c], Ewa Mijowska[c], Bernd Büchner[b], Silke Hampel[b], Nico Gräßler[b,*], Rüdiger Klingeler[a,*]

[a] *Kirchhoff Institute for Physics, Heidelberg University, 69120 Heidelberg, Germany*
[b] *Leibniz Institute for Solid State and Materials Research Dresden e.V., 01069 Dresden, Germany*
[c] *Nanomaterials Physicochemistry Department, Faculty of Chemical Technology and Engineering, West Pomeranian University of Technology, 71-065 Szczecin, Poland*
[d] *Department of Physics, Faculty of Science, Sohag University, 82524 Sohag, Egypt*

*Corresponding authors.
**Both authors contributed equally.
Email addresses: n.graessler@ifw-dresden.de (Nico Gräßler), klingeler@kip.uni.heidelberg.de (Rüdiger Klingeler)

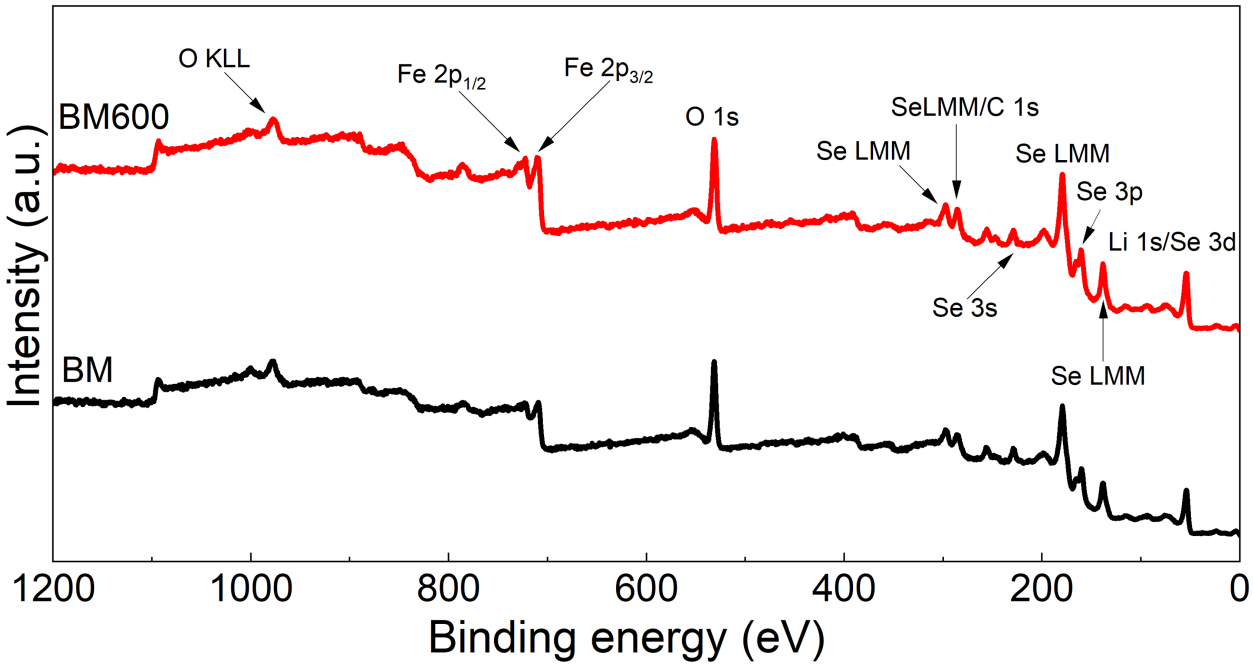

Figure S1 Full XPS spectra of (Li_2Fe)SeO-BM and (Li_2Fe)SeO-BM600

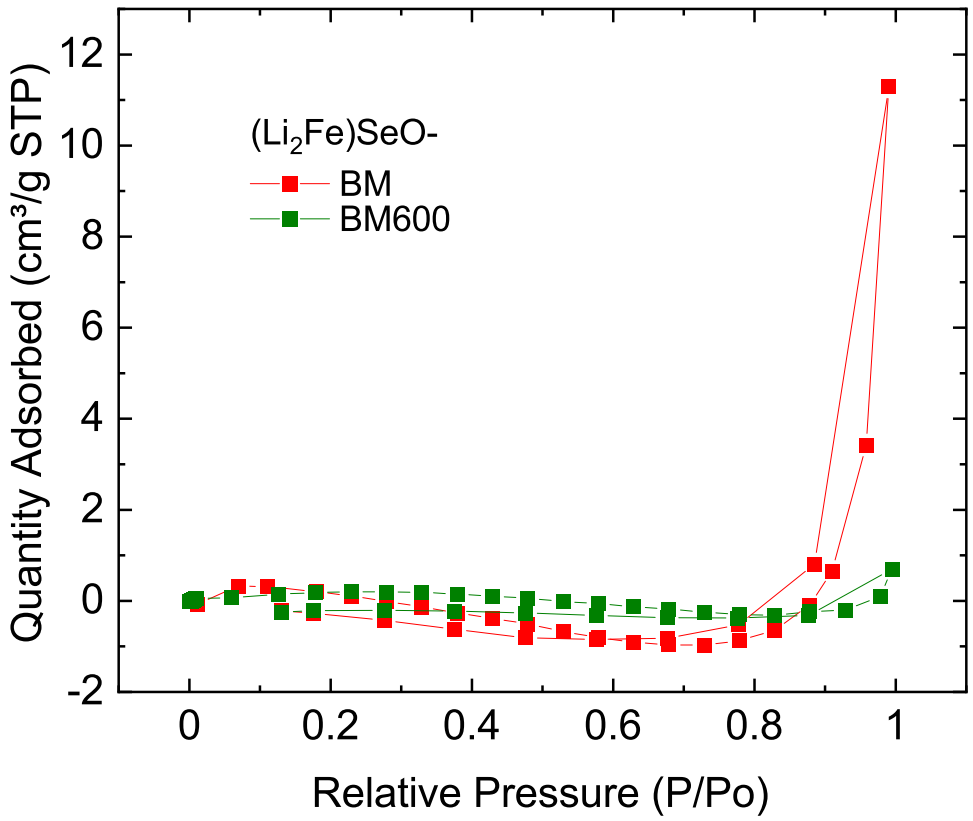

Figure S2 Nitrogen adsorption/desorption isotherms of $(Li_2Fe)SeO$-BM and $(Li_2Fe)SeO$-BM600.

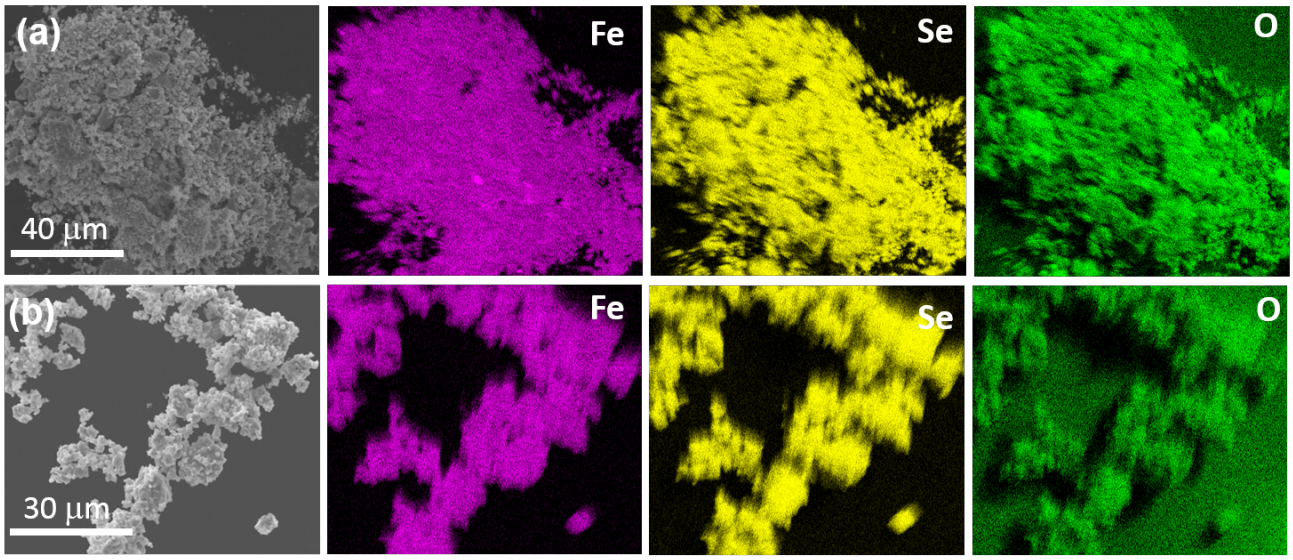

Figure S3 EDS mapping of iron, selenium and oxygen for $(Li_2Fe)SeO$-BM (a) and $(Li_2Fe)SeO$-BM600 (b). The two materials both possess a uniform distribution of the investigated elements.

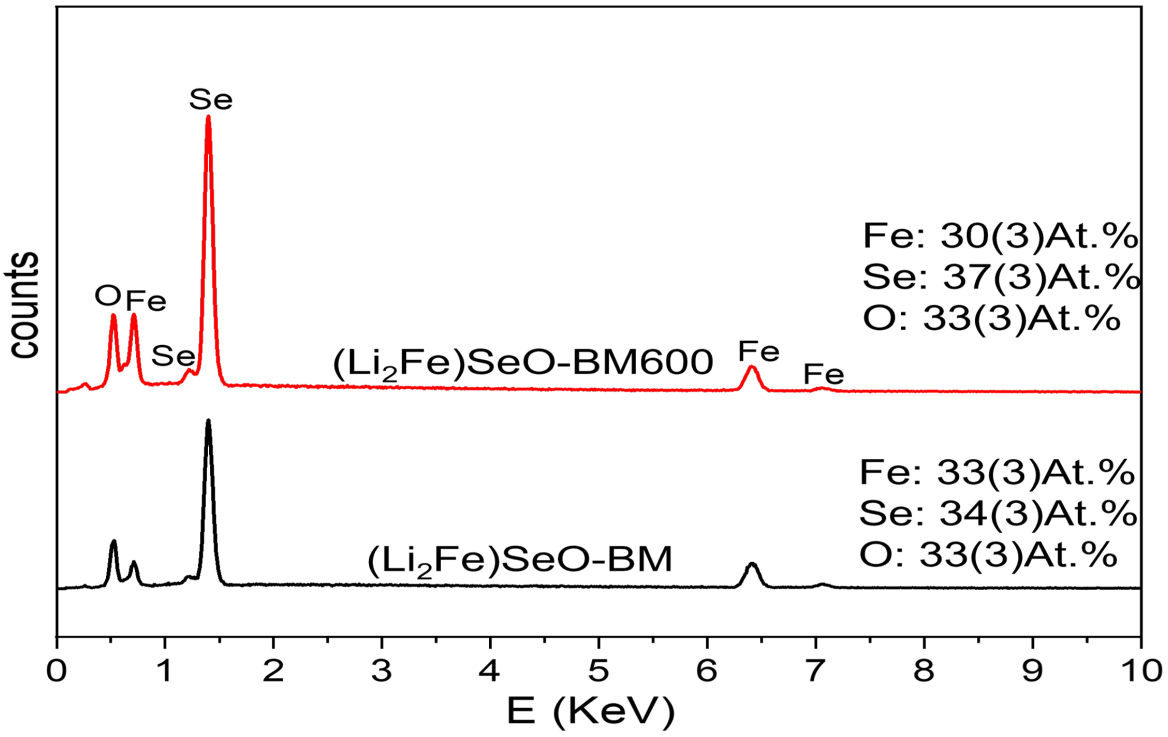

Figure S4 EDS spectra of $(Li_2Fe)SeO$-BM and $(Li_2Fe)SeO$-BM600 together with the atomic percent ratio of the existing elements. The results confirm within uncertainty the expected nominal composition of the materials.

Table S1 ICP-OES results for (Li_2Fe)SeO-BM and (Li_2Fe)SeO-BM600

compound	Mass %			Molar ratios[1]			
	Li	Fe	Se	Li	Fe	Se	O
(Li_2Fe)SeO-BM	8.36±0.13	33.92 ±0.49	47.87±0.55	1.971±0.031	0.994±0.014	0.992±0.011	1.043±0.003
(Li_2Fe)SeO-BM600	8.34±0.08	33.81±0.28	47.49±0.49	1.996±0.019	1.006±0.008	0.999±0.01	0.999±0.007

[1]Molar ratios are scaled to sum up to about 5

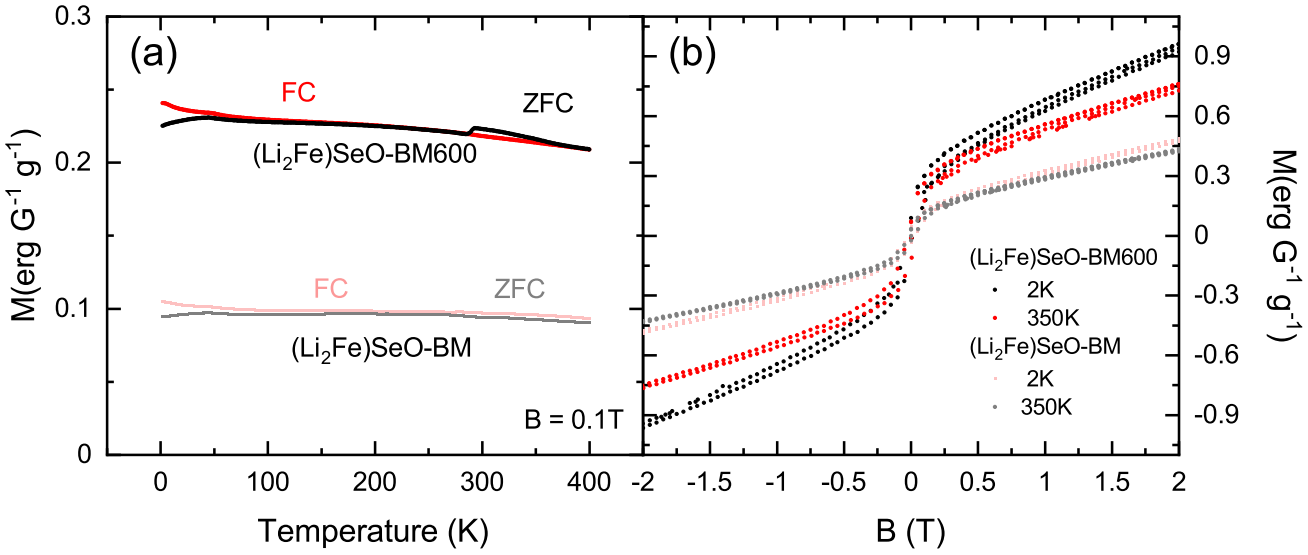

Figure S5 Magnetization of $(Li_2Fe)SeO$ vs. temperature at $B = 0.1$ T (a), and vs. magnetic field at $T = 2$ K (b). The data indicate a antiferromagnetic transition f at ($T_N \simeq 290$ K;) and a ferri or ferromagentic transition at 50 K. Hinting to the existence of $\beta-Fe_{1-x}Se$ with $x \approx 0.26$ and with $x \approx 0.21 - 0.29$ as impurity phase present [1, 2, 3].

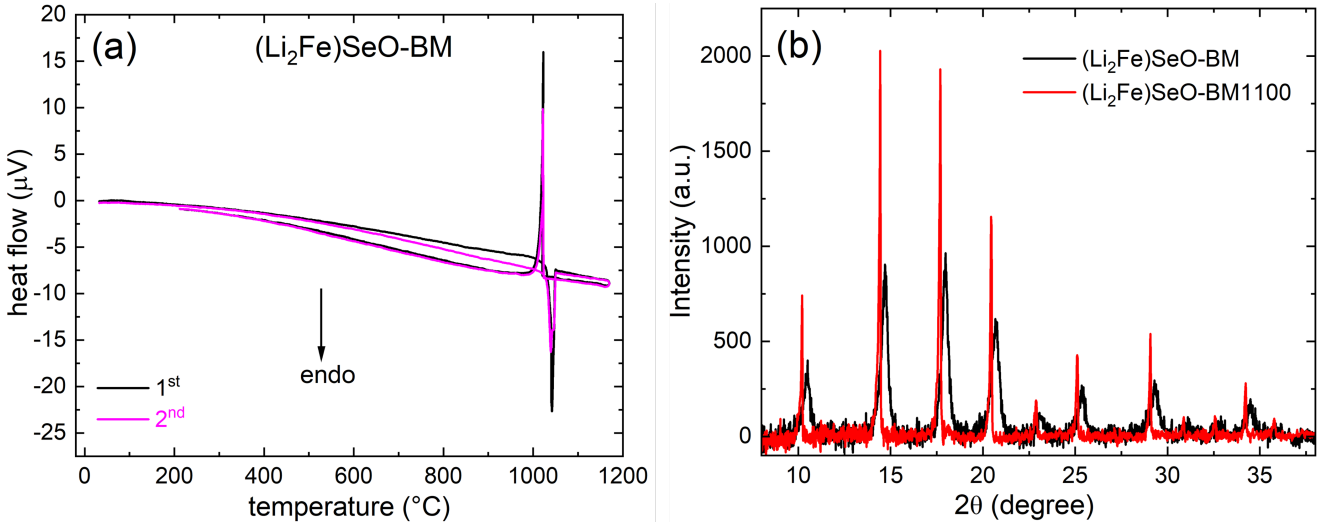

Figure S6 DTA for (Li_2Fe)SeO-BM (a) and XRD patterns (b) for pristine (Li_2Fe)SeO-BM and after its heat treatment at 1100 °C ((Li_2Fe)SeO-BM1100). To prove that no phase decomposition occurs, the (Li_2Fe)SeO-BM was heat-treated at 1100 °C (higher than its melting point) and then cooled normally to room temperature (we refer to this sample as ((Li_2Fe)SeO-BM1100). The XRD patterns using Mo $K_{\alpha 1}$ radiation source ($\lambda = 0.709300$ Å) show that by heating the sample above its melting point, the peaks increase in intensity and becomes sharper. This effect can be attributed to an improvement of crystallinity and long-range atomic order. In addition, a noticeable shift in the peaks position to lower 2θ angle is remarked, which corresponds to an expansion in the lattice parameter. The expansion of the lattice parameter may be attributed to strain relaxation and vanishing of the internal defects.

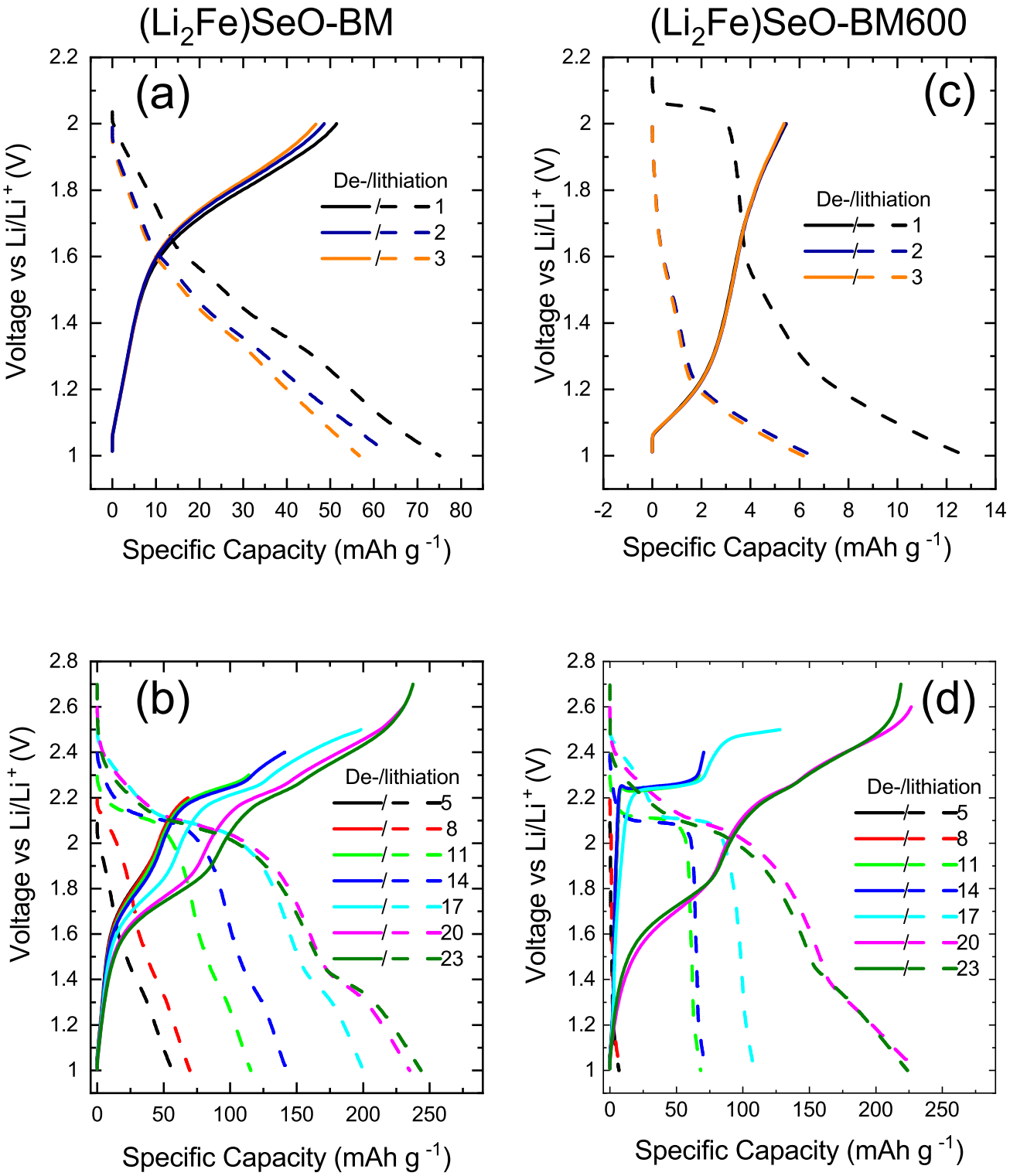

Figure S7 Potential profiles of $(Li_2Fe)SeO$-BM (a,b) and $(Li_2Fe)SeO$-BM600 (c,d) in specific potential ranges at a C/10 current rate. At each potential step, 3 discharge/charge cycles were recorded. At direct discharge $(Li_2Fe)SeO$-BM displays a pronounced capacity of around 75 mAh g^{-1} whereas $(Li_2Fe)SeO$-BM600 (c) shows a much lower capacity of around 12 mAh g^{-1} . By increasing the potential range in 0.1 V steps (b,d) a decisive increase of the low voltage feature R3/O3 is for both samples only visible at 2.6 V, leeding to a boundary voltage of 2.5 V.

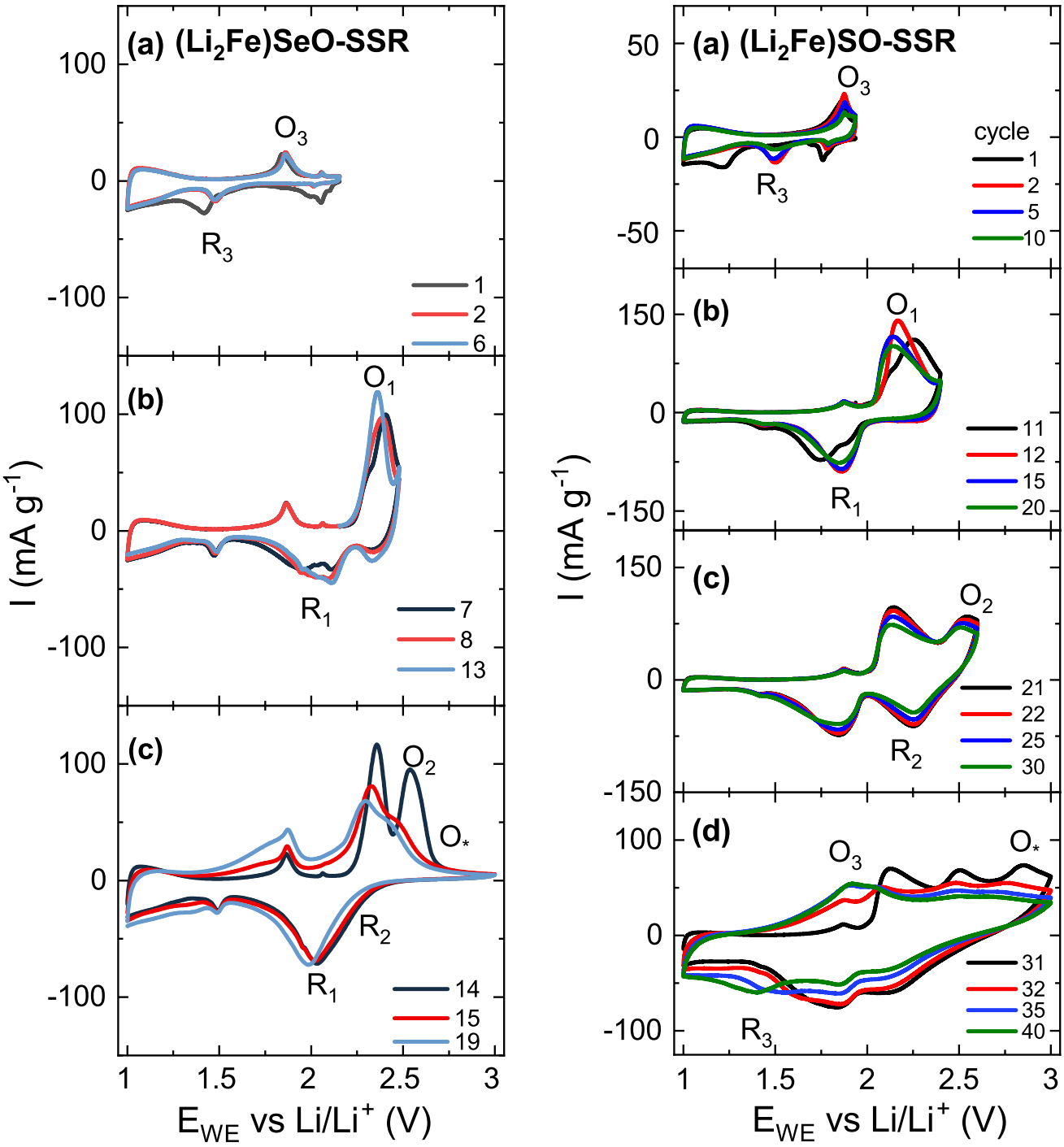

Figure S8 Cyclic voltammograms of (left) $(Li_2Fe)SeO$-SSR in the potential range from (a) 1 to OCV, (b) 1 to 2.4 V, (c) 1-3 V and (right) $(Li_2Fe)SO$-SSR in the potential range from (a) 1 to OCV, (b) 1 to 2.4 V, (c) 1 to 2.6 V and (d) 1 to 3 V vs Li/Li^+ measured at a scan rate of 0.1 mV s^{-1}. The cyclic voltammograms for both materials show, similar to the data shown for $(Li_2Fe)SeO$-BM and BM600 a pronounced increase in the low voltage O3/R3 feature only after the voltage range was extended and include the high voltage process O*. Note, the lower expression of O_3/R_3 after the first cycle for the $(Li_2Fe)SeO$-SSR samples compared to the ball-milled samples can likely be attributed to the much larger particles obtained through the SSR synthesis which reduces the number of active sites.

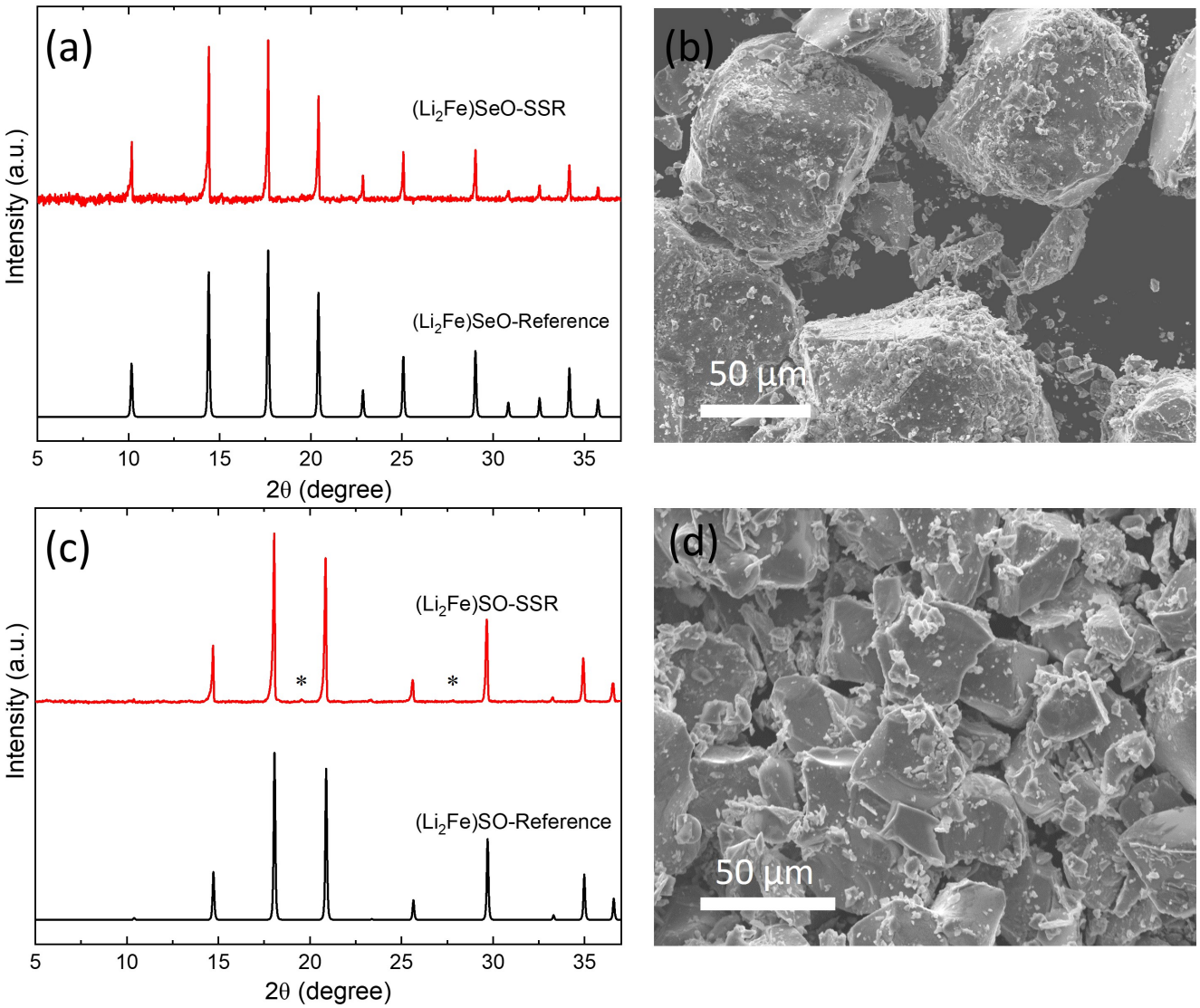

Figure S9 XRD (using Mo $K_{\alpha 1}$ radiation source ($\lambda = 0.709300$ Å)) and SEM image of $(Li_2Fe)SeO$ (a,b) and $(Li_2Fe)SO$ (c,d) prepared by solid-state reaction method. The synthesis was reproduced using the synthesis conditions from Ref.[4]. The asterisks in c refer to minor $LiFeO_2$ secondary phase.

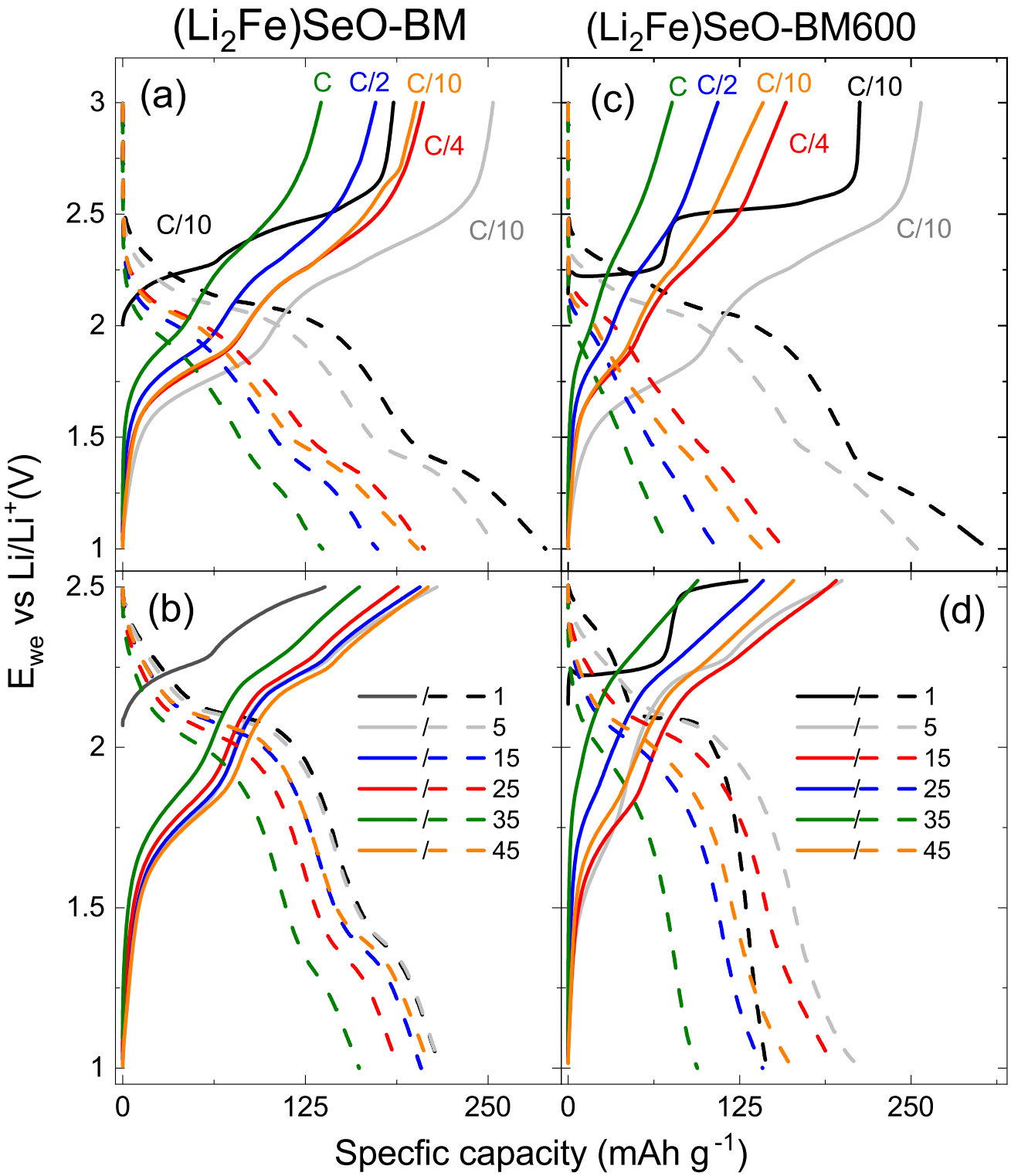

Figure S10 Potential profiles of (Li_2Fe)SeO-BM (a,b) and (Li_2Fe)SeO-BM600 (c,d) at different current rates of C/10, C/4, C/2 and C. The colors used symbolize distinct cycles and currents.

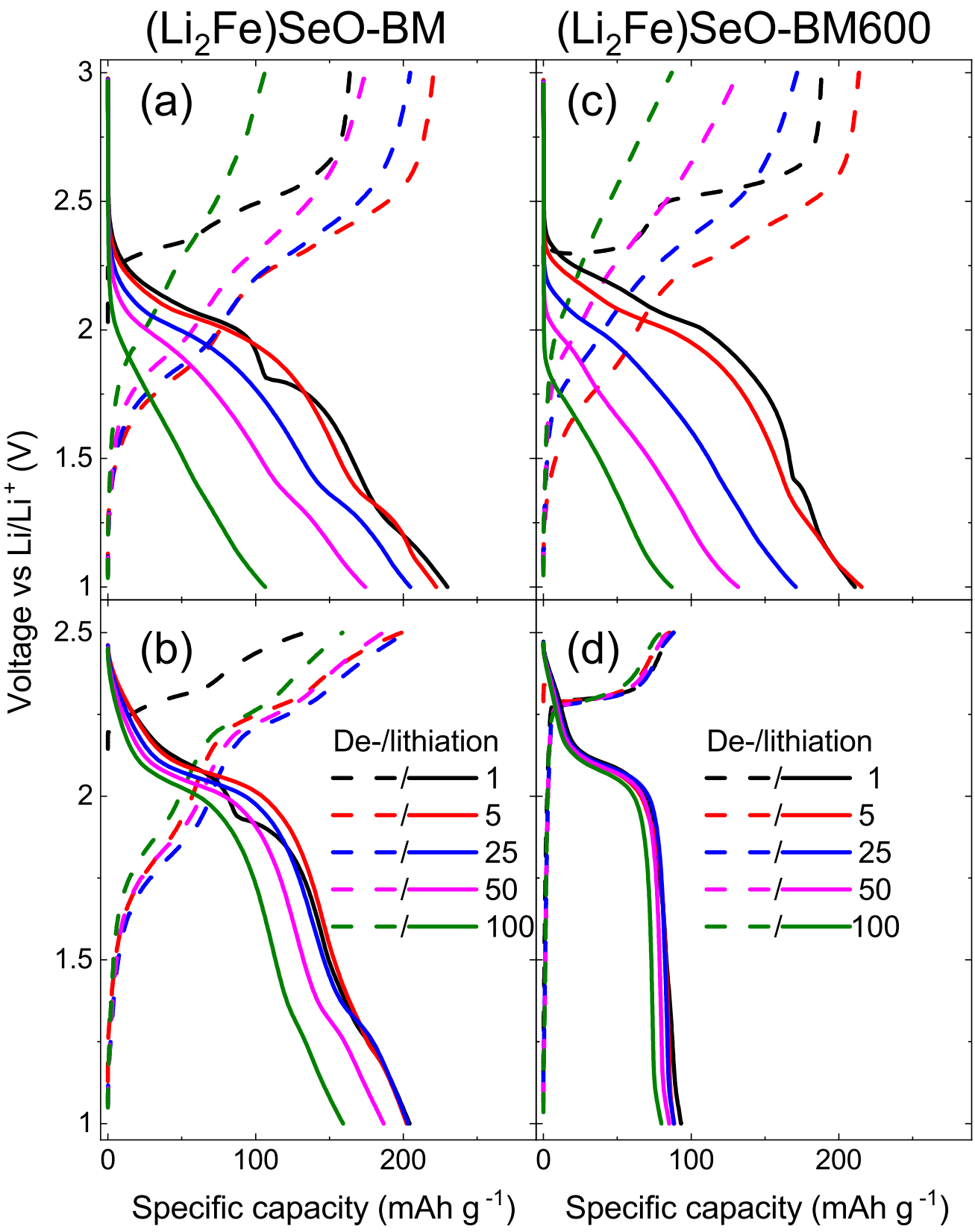

Figure S11 Potential profiles of (Li_2Fe)SeO-BM (a,b) and (Li_2Fe)SeO-BM600 (c,d) at a current rate of 1 C. The colors used symbolize distinct cycles.

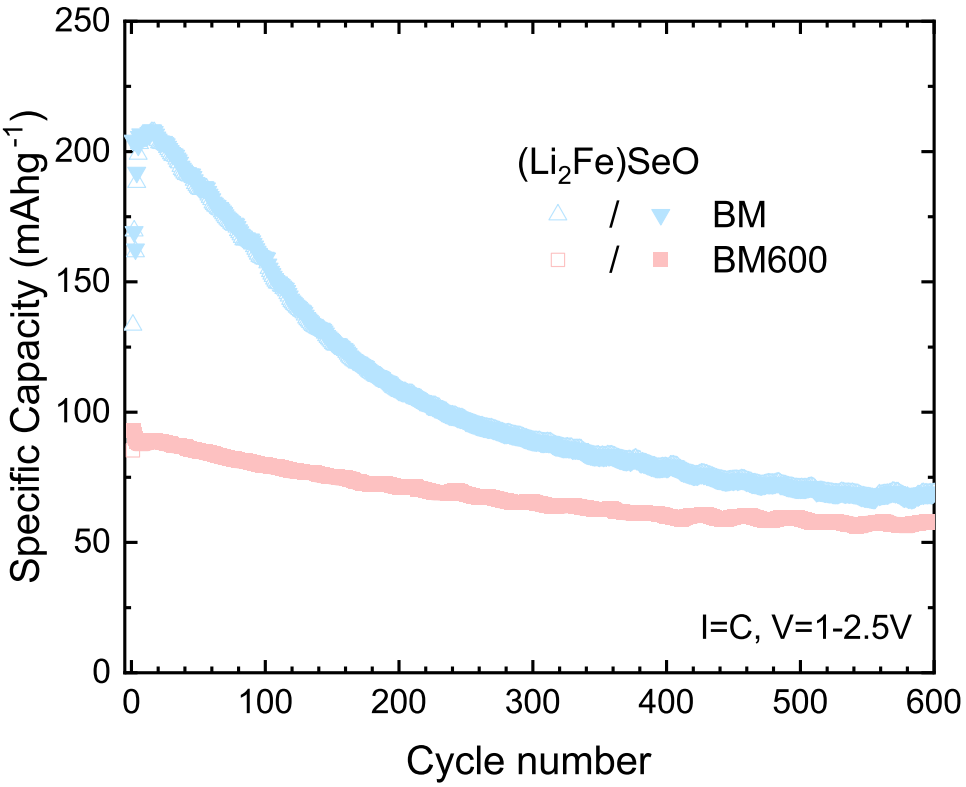

Figure S12 Longterm GCPL of $(Li_2Fe)SeO$-BM and $(Li_2Fe)SeO$-BM600 in the limited potential range from 1 to 2.5 V at 1C.

References

[1] P. Terzieff and K. L. Komarek, *Monatshefte für Chemie*, 1978, **109**, 1037–1047.
[2] T. Hirone, S. Maeda and N. Tsuya, *Journal of the Physical Society of Japan*, 1954, **9**, 496–499.
[3] P. Terzieff and K. L. Komarek, *Monatshefte fr Chemie*, 1978, **109**, 651–659.
[4] K. T. Lai, I. Antonyshyn, Y. Prots and M. Valldor, *Journal of the American Chemical Society*, 2017, **139**, 9645–9649.